esa

ECOSPHERE

Using ocean models to predict spatial and temporal variation in marine carbon isotopes

S. MAGOZZI,[1,3] A. YOOL,[2] H. B. VANDER ZANDEN,[3,4] M. B. WUNDER,[5] AND C. N. TRUEMAN[1,†]

[1]*School of Ocean and Earth Science, University of Southampton, European Way, Southampton SO14 3ZH UK*
[2]*National Oceanography Centre Southampton, European Way, Southampton SO14 3ZH UK*
[3]*Department of Geology and Geophysics, University of Utah, 115 S 1460 E, Salt Lake City, Utah 84112 USA*
[4]*Department of Biology, University of Florida, PO Box 118525, Gainesville, Florida 32611 USA*
[5]*Department of Integrative Biology, University of Colorado Denver, 1151 Arapahoe SI 2071, Denver, Colorado 80217 USA*

Citation: Magozzi, S., A. Yool, H. B. Vander Zanden, M. B. Wunder, and C. N. Trueman. 2017. Using ocean models to predict spatial and temporal variation in marine carbon isotopes. Ecosphere 8(5):e01763. 10.1002/ecs2.1763

Abstract. Natural-abundance stable isotope ratios provide a wealth of ecological information relating to food web structure, trophic level, and location. The correct interpretation of stable isotope data requires an understanding of spatial and temporal variation in the isotopic compositions at the base of the food web. In marine pelagic environments, accurate interpretation of stable isotope data is hampered by a lack of reliable, spatio-temporally distributed measurements of baseline isotopic compositions. In this study, we present a relatively simple, process-based carbon isotope model that predicts the spatio-temporal distributions of the carbon isotope composition of phytoplankton (here expressed as $\delta^{13}C_{PLK}$) across the global ocean at one degree and monthly resolution. The model is driven by output from a coupled physics-biogeochemistry model, NEMO-MEDUSA, and operates offline; it could also be coupled to alternative underlying ocean model systems. Model validation is challenged by the same lack of spatio-temporally explicit data that motivates model development, but predictions from our model successfully reproduce major spatial patterns in carbon isotope values observed in zooplankton, and are consistent with simulations from alternative models. Model predictions represent an initial hypothesis of spatial and temporal variation in carbon isotopic baselines in ocean areas where a few data are currently available, and provide the best currently available tool to estimate spatial and temporal variation in baseline isotopic compositions at ocean basin to global scales.

Key words: biogeochemistry; ecogeochemistry; food webs; geolocation; isoscapes; migration; modeling; natural chemical tags; pelagic; spatial ecology; trophic ecology; trophic position.

Received 27 October 2016; accepted 12 December 2016. Corresponding Editor: Jason B. West.

† **E-mail:** trueman@noc.soton.ac.uk

INTRODUCTION

Natural-abundance stable isotope analysis is a routine tool in ecology providing information on food web structuring, trophic interactions, and nutrient flux (e.g., Kelly 2000, Post 2002, Boecklen et al. 2011, Layman et al. 2012, Trueman et al. 2014, Choy et al. 2015), and offers a method for retrospective geolocation (e.g., Hobson 1999, Graham et al. 2010, Hobson et al. 2010, Wunder 2010, Trueman et al. 2012, 2016, Vander Zanden et al. 2015). All ecological applications of stable isotope data require consideration of spatial and temporal variation in the isotopic compositions of nutrients at the base of the food web, or in local precipitation in the case of stable oxygen and hydrogen isotopes. Incomplete knowledge of the likely spatio-temporal variation in baseline isotope values over an animal's foraging range, and/or over seasonal, annual, or multi-annual cycles, can lead to poor sampling design and inaccurate interpretation of results.

In terrestrial systems, continental- to global-scale isoscapes (sensu Bowen and West 2008, West et al. 2010, for a review, see Bowen 2010*a*) of stable hydrogen and oxygen isotope ratios in precipitation have been developed, based on the spatial interpolation of large numbers of spatio-temporally distributed isotopic measurements (e.g., Bowen and Revenaugh 2003, Bowen et al. 2005), and on statistical regression relationships between measured isotope values and environmental predictor variables such as latitude, altitude, temperature, and rainout (e.g., Meehan et al. 2004, Bowen 2010*b*). Over the past decade, geolocation methods using precipitation-based isoscapes have provided the foundation for a formidable body of migration science research in a range of terrestrial taxa, including insects, birds, and mammals (e.g., Wunder 2010, Van Wilgenburg and Hobson 2011, Hobson et al. 2012, Van Wilgenburg et al. 2012, Flockhart et al. 2013, Rundel et al. 2013, Cryan et al. 2014, Garcia-Perez and Hobson 2014).

In marine ecosystems, sampling of baseline isotope compositions is complicated by both highly dynamic biogeochemical cycles and a relatively inaccessible environment (for reviews, see Graham et al. 2010, Trueman et al. 2012, McMahon et al. 2013). Consequently, the use of stable isotope data in trophic and geolocation studies is particularly challenging in open marine environments. Stable hydrogen, oxygen, and strontium isotope ratios show relatively little spatial variation in seawater (Wassenaar 2008), but by contrast carbon ($\delta^{13}C$) and nitrogen ($\delta^{15}N$) isotope ratios show substantial spatio-temporal variations (e.g., Rau et al. 1989, Francois et al. 1993, Goericke and Fry 1994, Jennings and Warr 2003, Barnes et al. 2009, McMahon et al. 2013 and references therein). While carbon and nitrogen isoscapes are beginning to be developed in coastal and shelf areas (e.g., Jennings and Warr 2003, Barnes et al. 2009, Radabaugh et al. 2013, MacKenzie et al. 2014, Vokhshoori and McCarthy 2014, Vokhshoori et al. 2014, Vander Zanden et al. 2015, Trueman et al. 2016), a relatively few spatio-temporally explicit $\delta^{13}C$ and $\delta^{15}N$ datasets currently exist for open-ocean settings. Ocean basin-scale isoscapes have been constructed by spatial interpolation of published zooplankton $\delta^{13}C$ and $\delta^{15}N$ data (Graham et al. 2010, McMahon et al. 2013). However, such opportunistic compilations of literature data have relatively few, unevenly distributed data points (i.e., approximately 550 data points for the Atlantic Ocean; see McMahon et al. 2013), and consequently are strongly influenced by single data points or specific cruises. Furthermore, isotopic variation associated with season and year of sampling, taxa sampled, and processing methods cannot easily be controlled from opportunistic compilations of literature data.

In open-ocean settings, the application of stable isotopes to reconstruct broad-scale animal movements has been largely limited to high-latitude systems (e.g., Schell et al. 1989, Best and Schell 1996, Cherel et al. 2000, Cherel and Hobson 2007, Jaeger et al. 2010), where strong and predictable temperature-driven gradients dominate the spatial structure in baseline carbon isotopes (e.g., Rau et al. 1982, 1989, Dunton et al. 1989, Saupe et al. 1989, Francois et al. 1993, Schell et al. 1998). Realistic predictions of the spatio-temporal distributions of baseline isotope values across the global ocean would help to interpret the isotopic compositions of animal tissues in the context of marine spatial and trophic ecology, and aid the use of stable isotopes as geolocation tools for migratory oceanic animals (Graham et al. 2010, Ramos and Gonzalez-Solis 2012, Trueman et al. 2012, McMahon et al. 2013).

Coupled ocean physics–biogeochemistry models can provide a framework for mechanistic prediction of isotopic compositions of phytoplankton, and stable isotopes have been incorporated into several global system models (Hofmann et al. 2000, Tagliabue and Bopp 2008, Schmittner and Somes 2016). Access to full global ocean models is relatively restricted due to processing time, but output from model simulations is widely available. Here, we provide an offline extension to ocean ecosystem models predicting isotopic variability of carbon in phytoplankton based on parameters commonly simulated in global ocean biogeochemistry models.

Carbon isotope variation in phytoplankton

Spatial variations in the carbon isotope composition of phytoplankton ($\delta^{13}C_{PLK}$) co-vary with variations in sea surface temperature (Sackett et al. 1965, Fontugne and Duplessy 1981, Rau et al. 1982, 1989, Goericke and Fry 1994, Lara et al. 2010), concentration of dissolved CO_2 ($[CO_{2(aq)}]$; Rau et al. 1989, 1992, Goericke and Fry 1994, Rau

et al. 1997, Fischer et al. 1998), and phytoplankton physiology and community dynamics (Wong and Sackett 1978, Fry and Wainright 1991, Francois et al. 1993, Goericke et al. 1994, Bidigare et al. 1997, Popp et al. 1999, Maranon 2009, Lara et al. 2010). At high latitudes, regional- to global-scale patterns in $\delta^{13}C_{PLK}$ values strongly reflect sea surface temperature gradients, as temperature co-varies with direct drivers of isotopic fractionation, such as concentration of dissolved CO_2, phytoplankton growth rates, and community composition (see *Methods*). Values of $\delta^{13}C_{PLK}$ are increasingly decoupled from sea surface temperature at lower latitudes, where smaller, often seasonal changes in phytoplankton physiological correlates (e.g., growth rates and cell size) and community dynamics (e.g., community composition) may have greater influences than the relatively homogenous temperature. Concentration of dissolved CO_2, phytoplankton growth rates, cell size, and community composition act as direct controls on $\delta^{13}C_{PLK}$ values by influencing the degree of carbon isotope fractionation that occurs during photosynthesis (ε_p). In laboratory experiments, ε_p is positively related to the concentration of dissolved CO_2 (Hinga et al. 1994, Laws et al. 1995, 1997, Burkhardt et al. 1999) and negatively related to the specific growth rate of phytoplankton (μ; Laws et al. 1995, Bidigare et al. 1997, Laws et al. 1997, Burkhardt et al. 1999). The extent of isotopic fractionation occurring during photosynthetic carbon assimilation depends on the proportion of intracellular inorganic carbon that diffuses back into the surrounding water (Farquhar et al. 1982, Francois et al. 1993). Assuming that inorganic carbon enters the cell entirely *via* passive diffusion, this proportion is equivalent to the ratio of internal to external concentration of dissolved CO_2, which, in turn, is proportional to the specific growth rate of phytoplankton (Farquhar et al. 1982, Laws et al. 1995, 1997). Concentration of dissolved CO_2 in the environment is also controlled by phytoplankton growth rates, particularly during blooms (Freeman and Hayes 1992). In addition, because the flux of dissolved CO_2 into and out of the cell is also proportional to the ratio of cell volume to surface area, ε_p is negatively related to phytoplankton cell size, with large phytoplankton cells (e.g., diatoms) showing lower levels of isotopic fractionation (and thus more positive $\delta^{13}C$ values) than small-celled nanoplankton (Popp et al. 1998).

Based on the mechanisms described above, ε_p can be predicted from the concentration of dissolved CO_2, phytoplankton growth rates, size, and community composition. Given ε_p, and the isotopic composition of dissolved CO_2 ($\delta^{13}C_{CO2(aq)}$), $\delta^{13}C_{PLK}$ values can be estimated. Coupled circulation–biogeochemical ocean models can be used to estimate variables influencing carbon isotope fractionation at high spatial and temporal resolutions, and thus to predict $\delta^{13}C_{PLK}$ values at unmonitored sites and under dynamic environmental conditions (e.g., Hofmann et al. 2000, Tagliabue and Bopp 2008, Somes et al. 2010, Schmittner and Somes 2016). The choice of the underlying biogeochemical model should reflect a compromise between relatively simple models with a few variables (i.e., degrees of freedom), and more complex models with potentially increased accuracy but also increased computing demand and more opaque relationships between the underlying assumptions and the output.

Here, we use an ocean general circulation model (GCM) coupled to a biogeochemistry model of intermediate complexity, NEMO-MEDUSA (Madec and the NEMO team 2008, Yool et al. 2013), combined with general assumptions related to carbon isotope fractionation, to develop a relatively simple, offline, process-based carbon isotope model; this model predicts the spatio-temporal distributions of $\delta^{13}C_{PLK}$ values across the global surface ocean at one degree and monthly resolution. This isotopic extension could be coupled to any existing earth system model that generates predictions of sea surface temperature, concentration of CO_2 and other components within the dissolved inorganic carbon (DIC) pool, and phytoplankton growth rates and proportional abundance.

Based on the underlying mechanisms of isotopic variation included in the model, as well as on observed patterns of variation in nature (e.g., Rau et al. 1989, Francois et al. 1993, Goericke and Fry 1994, Goericke et al. 1994, McMahon et al. 2013), we expect (1) basin- to global-scale variations in simulated $\delta^{13}C_{PLK}$ values to be largely driven by large-scale changes in the concentration and isotopic composition of CO_2, as well as growth rates and proportional abundance of key phytoplankton functional groups, and thus to co-vary with sea surface temperature, (2) regional-scale variations in $\delta^{13}C_{PLK}$ values to be super-imposed on broad latitudinal isotopic

gradients, and caused by smaller, often seasonal changes in phytoplankton physiological correlates and community dynamics, and (3) highest temporal variability in $\delta^{13}C_{PLK}$ values to occur in regions characterized by strong, transient phytoplankton blooms (e.g., high/temperate latitudes and upwelling regions) and by periodical oceanographic and/or climatic phenomena.

Methods

NEMO-MEDUSA

We used the coupled physics–biogeochemistry model, NEMO-MEDUSA, to generate global-scale fields of relevant properties (sea surface temperature, concentration of dissolved CO_2, growth rates, and proportional abundance of key phytoplankton functional groups) to estimate the carbon isotope fractionation occurring during photosynthesis (for fractionation occurring within the DIC pool, and during air–sea CO_2 exchange, see Appendix S1). The physical component of this model, NEMO (Nucleus for the European Modelling of the Ocean; Madec and the NEMO team 2008), is a GCM, including a sea-ice submodel (LIM2; Timmermann et al. 2005), configured here at approximately 1° horizontal resolution, with vertical space divided into 64 levels with thicknesses increasing from 6 m at the surface to 250 m at 6000 m. The biogeochemical component, MEDUSA-2.0 (Model of Ecosystem Dynamics, nutrient Utilization, Sequestration and Acidification; Yool et al. 2013), is an intermediate complexity ecosystem model founded on the elemental cycles of nitrogen, carbon, silicon, and iron. NEMO-MEDUSA has been extensively described and validated (for a complete description, see Yool et al. 2013); thus, here we only report information relevant to the development of the carbon isotope model.

In brief, NEMO-MEDUSA assigns phytoplankton to two functional groups: large-celled "diatoms" and small-celled "non-diatoms," which are intended to represent micro- and pico-phytoplankton, respectively. Phytoplankton growth is limited by temperature, light, and nutrient (nitrogen and iron) availability, with "diatoms" being additionally constrained by silicon availability. Within NEMO-MEDUSA, DIC is always available in excess to phytoplankton and is, therefore, entirely assimilated *via* passive diffusion in the form of $CO_{2(aq)}$, although in reality some phytoplankton groups may also actively take up HCO_3^- and CO_3^{2-}, particularly when $CO_{2(aq)}$ is limiting (see Keller and Morel 1999). NEMO-MEDUSA variables (nutrients, phytoplankton, zooplankton, and detritus) are simulated for the full 3D water column, but the outputs used in the carbon isotope model (Table 1) are taken from the top ~6 m of the ocean's surface, with the exception of phytoplankton growth rates and biomass, which are mixed-layer averages.

NEMO-MEDUSA was run for the period 1860–2100 under atmospheric forcing (temperature, humidity, winds, downward heat, and freshwater fluxes) derived from a simulation of the HadGEM2-ES climate model performed as part of Phase 5 of the Coupled Model Intercomparison Project (CMIP5; Collins et al. 2011, Jones et al. 2011). This simulation used the historical atmospheric pCO_2 record to 2005, then Representative Concentration Pathway 8.5 out to 2100. The use of such model-derived forcing means that patterns of variability will not exactly match that observed for particular years since the models contain their own internal variability.

For our analysis, we used outputs for the period 2001–2010 at monthly resolution, and re-gridded these onto the standard World Ocean Atlas grid (regular 1° × 1° resolution). To avoid influences from particular years, we averaged outputs for the period 2001–2010 to create a monthly climatology (i.e., of 10 yr of Januarys, Februarys), and then used this climatology to calculate a single annual average and a single intra-annual range (over all averaged months) in $\delta^{13}C_{PLK}$ values. Results of annual average $\delta^{13}C_{PLK}$ values over individual model years for the period 2001–2010 are also presented in Appendix S2. In addition, we calculated inter-annual range in $\delta^{13}C_{PLK}$ values as the range of annual average values over individual model years for the period 2001–2010.

$\delta^{13}C_{PLK}$ parameterization

We defined $\delta^{13}C_{PLK}$ as the difference between the isotopic composition of the substrate $CO_{2(aq)}$ ($\delta^{13}C_{CO2(aq)}$; for parameterization, see Appendix S1) and the overall carbon isotope fractionation occurring during photosynthesis (ε_p; Freeman and Hayes 1992). Indeed, ε_p is the major source of variability in $\delta^{13}C_{PLK}$ (Rau et al. 1982, 1989), although carbon isotope fractionation within the

Table 1. The NEMO-MEDUSA variables and other literature-derived parameters used as inputs in the carbon isotope model.

Terms	Source	Category	Layer	Value	Unit (MEDUSA)
Sea Surface Temperature (SST)	MEDUSA	Dynamic	Surface	Variable	°C
Concentration of Dissolved Inorganic Carbon (DIC)	MEDUSA	Dynamic	Surface	Variable	$mmol/m^3$
Concentration of CO_3^{2-} ($[CO_3^{2-}]$)	MEDUSA	Dynamic	Surface	Variable	$mmol/m^3$
Diatom growth rate (μ_d)	MEDUSA	Dynamic	Mixed layer	Variable	s^{-1}
Non-diatom growth rate (μ_n)	MEDUSA	Dynamic	Mixed layer	Variable	s^{-1}
Concentration of $CO_{2(aq)}$ ($[CO_{2(aq)}]$)†	MEDUSA	Dynamic	Surface	Variable	mol/m^3
Diatom biomass	MEDUSA	Dynamic	Mixed layer	Variable	mmol N m^2
Non-diatom biomass	MEDUSA	Dynamic	Mixed layer	Variable	mmol N m^2
Diatom cell radius (r_d)	Maranon (2009)	Fixed	n.a.	5×10^{-6}	m
Non-diatom cell radius (r_n)	Maranon (2009)	Fixed	n.a.	1×10^{-6}	m
Diatom cell surface (S_d)	Rau et al. (1996, 1997)	Fixed	n.a.	$4 \times \pi \times r_d^2$	m^2
Non-diatom cell surface (S_n)	Rau et al. (1996, 1997)	Fixed	n.a.	$4 \times \pi \times r_n^2$	m^2
Diatom cell volume (V_d)	Rau et al. (1996, 1997)	Fixed	n.a.	$4/3 \times \pi \times r_d^3$	m^3
Non-diatom cell surface (S_n)	Rau et al. (1996, 1997)	Fixed	n.a.	$4/3 \times \pi \times r_n^3$	m^3
Diatom cell carbon content (γ_d)	Rau et al. (1996, 1997)	Fixed	n.a.	$3.154 \times 10^{-14} \times V_d(\mu m^3)^{0.758}$	mol C
Non-diatom cell carbon content (γ_n)	Rau et al. (1996, 1997)	Fixed	n.a.	$3.154 \times 10^{-14} \times V_n(\mu m^3)^{0.758}$	mol C
Enzymatic fractionation during intracellular C fixation (ε_f)	Rau et al. (1996, 1997)	Fixed	n.a.	25	‰
Diffusive fractionation of $CO_{2(aq)}$ in seawater (ε_d)	Rau et al. (1996, 1997)	Fixed	n.a.	0.7	‰
Temperature-sensitive diffusivity of $CO_{2(aq)}$ in seawater (D_t)	Rau et al. (1996, 1997)	Fixed	n.a.	1.45×10^{-9}	m^2/s
Reacto-diffusive length (r_k)	Rau et al. (1996, 1997)	Fixed	n.a.	2.06×10^{-4}	m
Cell wall permeability to $CO_{2(aq)}$ (P)	Rau et al. (1996, 1997)	Fixed	n.a.	10^{-4}	m/s

Notes: The NEMO-MEDUSA variables are dynamic and, in general, were simulated for the ocean's surface, with the exception of phytoplankton growth rates and biomass, which were mixed-layer averages. Literature-derived parameters are fixed and, in general, were assigned base values from Rau et al. (1996, 1997), with the exception of "diatom" and "non-diatom" cell radii, which were assigned base values from Maranon (2009). The units in which model variables or fixed parameters are expressed in the model are also reported.

† While NEMO-MEDUSA does not distinguish between the concentration of dissolved CO_2 ($[CO_{2(aq)}]$) and the concentration of carbonic acid ($[H_2CO_3]$), $[H_2CO_3]$ in seawater is negligible in comparison to $[CO_{2(aq)}]$ (Zeebe et al. 1999).

DIC pool and during air–sea CO_2 exchange also contributes, to an extent, to variation in $\delta^{13}C_{PLK}$ (i.e., through influencing $\delta^{13}C_{CO2(aq)}$), and thus is also parameterized in the carbon isotope model (see Appendix S1). Diazotrophs are not modeled explicitly within NEMO-MEDUSA, but some diazotrophs such as *Trichodesmium* are known to display relatively low levels of isotopic fractionation, and thus more positive $\delta^{13}C$ values (Carpenter et al. 1997). We therefore make an assumption that diazotroph contribution to total phytoplankton carbon is relatively minor.

Photosynthetic carbon isotope fractionation.—We calculated the overall photosynthetic carbon isotope fractionation in each month (ε_p) as the average fractionation of small-celled, and silica-limited large-celled phytoplankton (i.e. "diatoms" and "non-diatoms," respectively), weighted by their proportional abundance. In this instance, we parameterized the photosynthetic carbon isotope fractionation of the phytoplankton group i (ε_{pi}) as a linear function of $[CO_{2(aq)}]$, used as a proxy for carbon supply, and the specific growth rate of the phytoplankton group i (μ_i), used as a proxy

for carbon demand (Farquhar et al. 1982, Laws et al. 1995); we used the same parameterization of ε_{pi} as Rau et al. (1996, 1997) (Eq. 1):

$$\varepsilon_{pi} = \varepsilon_f + \frac{b_i}{\left[CO_{2(aq)}\right]};$$
$$b_i = -(\varepsilon_f - \varepsilon_d)\frac{\gamma_i \times \mu_i}{S_i}\left(\frac{r_i}{D_t \times \left(1 + \frac{r_i}{r_k}\right)} + \frac{1}{P}\right) \quad (1)$$

where the terms $[CO_{2(aq)}]$ and μ_i (i.e., concentration of $CO_{2(aq)}$ and specific growth rate of the phytoplankton group i, respectively) are NEMO-MEDUSA outputs, and all the other terms are fixed values (Table 1).

We fixed the cell radius (r_i) at 50 μm for "diatoms" and at 10 μm for "non-diatoms" (Maranon 2009 and references therein); the cell surface area (S_i) and volume (V_i) depended on r_i, and the cell carbon content (γ_i), in turn, on V_i. We assigned base values from Rau et al. (1996, 1997) to enzymatic isotope fractionation associated with intracellular carbon fixation (ε_f), diffusive isotope fractionation of $CO_{2(aq)}$ in seawater (ε_d), temperature-sensitive diffusivity of $CO_{2(aq)}$ (D_t), reacto-diffusive length (r_k), and cell wall permeability (P). Additionally, to account for the influence of cell size and geometry on ε_{pi} (Popp et al. 1998), and to replicate the observed minimum of ε_{pi} at high values of $\mu_i/[CO_{2(aq)}]$ (Laws et al. 1995, 1997), we constrained ε_{pi} between 5‰ and 20‰ and between 10‰ and 26‰ for "diatoms" and "non-diatoms," respectively (see Tagliabue and Bopp 2008).

Day-length correction, scaling, and latitude-dependent limitation of phytoplankton growth rates.—Ocean biogeochemical–ecosystem models frequently struggle to derive growth rate terms consistent with satellite estimates (Schmittner et al. 2013). Phytoplankton growth rates estimated by NEMO-MEDUSA represent the average growth over 24 h, while growth rates measured in the laboratory—and used to constrain Eq. 1—reflect the proportion of growth during the photoperiod (i.e., specific growth rate, μ; Laws et al. 1995, 1997, see also Rau et al. 1996, 1997). To convert NEMO-MEDUSA average growth rates to specific growth rates, therefore, we applied a day-length correction depending on latitude and month (Forsythe et al. 1995). Growth rates in NEMO-MEDUSA integrate growth throughout the mixed layer, whereas laboratory-derived growth rates in Eq. 1 were equivalent to growth at the surface (Laws et al. 1995, 1997, see also Rau et al. 1996, 1997). To provide comparable growth rate units, we scaled NEMO-MEDUSA specific growth rates by a power-law conversion (Eq. 2).

$$u_{i-scaled} = \beta \times u_i^{\alpha}, \quad (2)$$

where β = 1.5 and 2.00, and α = 0.2 and 0.3 for "diatoms" and "non-diatoms," respectively. Values of the β coefficient constrain maximum specific growth rate to ~1.5 and 2 cell divisions d^{-1} for "diatoms" and "non-diatoms," respectively.

The NEMO-MEDUSA model systematically under-estimates phytoplankton growth rates and biomass in oligotrophic regions, attributed in part to the assumption of geographically invariant nutrient kinetics, which does not permit phytoplankton to adapt to oligotrophic conditions (Yool et al. 2013). Therefore, at latitudes between 40° N and 40° S, we set growth rate lower limits to 1.25 and 1.75 cell divisions d^{-1} for "diatoms" and "non-diatoms," respectively; at latitudes polewards of 60° N and 60° S, we set lower limits to 1 cell divisions d^{-1} for both phytoplankton groups. Optimal values of the α and β coefficients for the power-law conversion, cell radii, and latitude-dependent growth rate lower limits were defined to ensure that predicted values remained in the range of $\delta^{13}C$ data for zooplankton provided by McMahon et al. (2013).

Isoscape development

The carbon isotope model estimates the surface water distribution of $\delta^{13}C_{PLK}$ values at one degree and monthly resolution. To reduce the effect of seasonal and decadal variability on $\delta^{13}C_{PLK}$ values, and provide isoscapes more relevant to higher-trophic-level animals assimilating carbon into tissues over longer time scales (Goering et al. 1990, Bump et al. 2007; see *Discussion*), we estimated the annually averaged surface water distribution of $\delta^{13}C_{PLK}$ values. To do this, we calculated annual average ε_p as the mean of monthly ε_p values of "diatoms" and "non-diatoms," weighted by their proportional contribution to the total annual phytoplankton production. We estimated annual average $\delta^{13}C_{CO2(aq)}$ values simply as the mean of monthly $\delta^{13}C_{CO2(aq)}$ values. In addition, to provide an estimate of the temporal variability in baseline carbon isotopes, we estimated the intra- and inter-annual range in $\delta^{13}C_{PLK}$ values.

Annual average and intra-annual range in $\delta^{13}C_{PLK}$ values, as well as annual average $\delta^{13}C_{CO2(aq)}$ values, are estimated using a monthly climatology for the period 2001–2010, while inter-annual range in $\delta^{13}C_{PLK}$ values is calculated as the range of annual average $\delta^{13}C_{PLK}$ over individual model years for the period 2001–2010.

We displayed annual average and intra- and inter-annual range in $\delta^{13}C_{PLK}$ values as continuous surfaces, within nine (annual average and range, respectively) discrete clusters of "similar" $\delta^{13}C_{PLK}$ values defined a posteriori according to model-based cluster analysis (R function *mclust*; Fraley et al. 2012), and within 54 biogeographic provinces defined a priori by Longhurst (1995, 1998, 2006). Given the simplifications and assumptions inherent in the carbon isotope model, discrete isoscape maps may represent the spatio-temporal variability in $\delta^{13}C_{PLK}$ values at resolutions more realistic than one degree, and at scales more relevant to the movements of migratory oceanic animals.

Validation

Rigorous validation of model isoscapes is challenged by the same lack of spatio-temporally explicit reference isotope data that encourage their development (Graham et al. 2010, Trueman et al. 2012, McMahon et al. 2013). The most comprehensive compilation of surface ocean $\delta^{13}C$ data is available from McMahon et al. (2013) for zooplankton (i.e., $\delta^{13}C_{ZPLK}$) within the Atlantic Ocean, which we used to tune model parameters as described above. As there are insufficient published $\delta^{13}C$ data to create comparative global continuous surface isoscapes, we divided the global ocean according to Longhurst biogeographic provinces (Longhurst 1995, 1998, 2006), and calculated the mean modeled annual average $\delta^{13}C$ value and its associated standard deviation within each province. We then assembled available literature $\delta^{13}C_{ZPLK}$ data across the global ocean, and estimated mean measured $\delta^{13}C_{ZPLK}$ values within 49 of the 54 discrete provinces (Table 2). For each study, we calculated a mean $\delta^{13}C$ value for zooplankton samples recovered within discrete regions. We averaged across the individual study means to estimate mean and variance for $\delta^{13}C_{ZPLK}$ values in each sampled province. We compared modeled and measured values using Monte Carlo resampling and simple linear regression. For each of 500 iterations, we randomly selected 33 of the 49 provinces (67% of cases) and, for each province, drew from the modeled and measured distribution of available $\delta^{13}C$ values. We estimated the intercept, slope, and R^2 values, and residual standard error associated with the regression model for each iteration, and reported the resulting mean or median of these regression coefficients across the 500 iterations.

We also conducted a cross-model validation exercise. Alternative models predicting $\delta^{13}C_{PLK}$ values have been described, based on different underlying ocean biogeochemical model constructs. Schmittner et al. (2013) and Schmittner and Somes (2016) incorporated carbon and nitrogen isotopes into the UVic Earth System Model. In this framework, carbon isotopes are explicitly modeled throughout the ocean carbon cycle, but phytoplankton growth rates are not included in the calculation of isotopic fractionation during photosynthesis.

Results

Spatial patterns in $\delta^{13}C_{PLK}$ values

Predicted annual average $\delta^{13}C_{PLK}$ values range between −31‰ and −16.5‰ across the global ocean (Fig. 1); the mean ± SD predicted annual average $\delta^{13}C_{PLK}$ value is −23.4‰ ± 3.7‰ for the global ocean. On basin to global scales, annual average $\delta^{13}C_{PLK}$ values vary across broad latitudinal gradients, showing steeper variation at high and temperate latitudes than in the tropics. Between 30° N and 30° S, annual average $\delta^{13}C_{PLK}$ values are relatively uniform and positive, varying between −24.5‰ and −16.5‰ (mean ± SD: −19.9‰ ± 1.4‰), with peaks of −18‰ to −16‰ in equatorial upwelling regions. Annual average $\delta^{13}C_{PLK}$ values decrease rapidly from latitudes polewards of 30° N and 30° S, varying between −29‰ and −17‰ in the subtropics and temperate latitudes, with most positive values of −22‰ to −20‰ at the subtropical convergence, in upwelling regions and the Gulf Stream current. At latitudes >60° in the Northern Hemisphere, annual average $\delta^{13}C_{PLK}$ values range between −30‰ and −27‰ (mean ± SD: −29.0‰ ± 0.6‰), with most positive values of −27‰ in the Norwegian Sea and most negative values of −29‰ to −30‰ in the Chukchi and Beaufort seas. At comparable latitudes in the Southern Hemisphere, annual average $\delta^{13}C_{PLK}$ values vary between −31‰ and −23‰

Table 2. Literature compilation of $\delta^{13}C$ data for zooplankton ($\delta^{13}C_{ZPLK}$) and modeled $\delta^{13}C_{PLK}$ data across Longhurst biogeographic provinces (Longhurst 1995, 1998, 2006).

Longhurst biogeographic province	Measured mean $\delta^{13}C_{ZPLK}$	Measured SD $\delta^{13}C_{ZPLK}$	Reference(s)	Modeled mean $\delta^{13}C_{PLK}$	Modeled SD $\delta^{13}C_{PLK}$	Modeled total range $\delta^{13}C_{PLK}$
Polar—Boreal Polar Province (POLR)	−23.0	1.4	1,2,3,23,24	−27.4	1.1	6.6
Polar—Atlantic Arctic Province	−23.4	1.5	2,5	−26.0	1.0	4.4
Polar—Atlantic Subarctic Province	−23.7	0.9	2,6	−25.0	1.1	4.8
Westerlies—N. Atlantic Drift Province (WWDR)	−21.3	0.0	2	−23.5	1.2	4.2
Westerlies—Gulf Stream Province	−21.1	0.0	2	−20.3	1.1	5.1
Westerlies—N. Atlantic Subtropical Gyral Province (West) (STGW)	−21.2	0.7	2	−20.4	0.9	3.6
Trades—N. Atlantic Tropical Gyral Province (TRPG)	−20.4	0.3	2,4	−20.9	1.1	4.8
Trades—Western Tropical Atlantic Province	−19.6	0.4	2,4	−19.2	0.4	1.7
Trades—Eastern Tropical Atlantic Province	−21.5	0.0	2,7	−19.0	0.5	2.7
Trades—South Atlantic Gyral Province (SATG)	−20.9	0.0	2	−21.6	1.3	5.2
Coastal—NE Atlantic Shelves Province	−21.5	0.5	2,8,9,10	−23.9	1.4	6.7
Coastal—Canary Coastal Province (EACB)	−20.4	0.9	2,7	−20.1	1.5	4.6
Coastal—Guianas Coastal Province	−18.3	0.0	2	−19.4	0.6	3.2
Coastal—NW Atlantic Shelves Province	−21.6	0.5	2	−23.3	2.0	6.2
Westerlies—Mediterranean Sea. Black Sea Province	−21.6	2.3	2,11,12,13	−23.5	0.3	2.7
Trades—Caribbean Province	−21.0	0.7	2	−20.0	0.7	2.9
Westerlies—N. Atlantic Subtropical Gyral Province (East) (STGE)	−21.8	0.5	2,14	−22.3	1.2	4.6
Coastal—Brazil Current Coastal Province	−19.6	1.3	2	−21.4	1.5	5.8
Coastal—SW Atlantic Shelves Province	−22.9	0.0	2	−23.6	1.8	7.6
Coastal—Benguela Current Coastal Province	−19.4	0.0	7	−19.1	0.5	1.9
Trades—Indian Monsoon Gyres Province	−20.1	0.0	51	−18.4	0.4	2.3
Trades—Indian S. Subtropical Gyre Province	−20.5	1.3	15,16,18,51	−21.0	1.4	5.2
Coastal—E. Africa Coastal Province	−19.3	0.8	17,19	−19.4	0.7	4.4
Coastal—Red Sea. Persian Gulf Province	−19.8	1.1	18,20,21	−20.8	1.0	3.3
Coastal—NW Arabian Upwelling Province	−19.8	0.9	18,22	−18.4	0.5	2.7
Coastal—E. India Coastal Province	−19.6	0.0	18	−17.8	0.2	0.9
Coastal—W. India Coastal Province	−19.7	0.6	51	−18.4	0.3	1.4
Polar—N. Pacific Epicontinental Province	−21.7	0.5	23,24	−25.6	1.7	9.2
Westerlies—Pacific Subarctic Gyres Province (East)	−22.0	0.0	3	−24.7	0.8	4.3
Westerlies—Pacific Subarctic Gyres Province (West)	−22.5	1.0	24	−25.6	0.9	4.1
Westerlies—Kuroshio Current Province	−20.7	1.9	26,27,28,29,30	−19.9	1.0	5.0
Westerlies—N. Pacific Polar Front Province	−21.8	2.3	3,23,31	−22.6	1.1	5.1
Westerlies—S. Pacific Subtropical Gyre Province	−23.3	1.7	25	−21.2	1.3	5.1
Trades—N. Pacific Tropical Gyre Province	−18.6	1.2	32,49	−21.6	1.8	6.3
Trades—N. Pacific Equatorial Countercurrent Province	−20.2	1.7	25,33,34,35,36	−18.8	0.4	2.3
Trades—Pacific Equatorial Divergence Province	−20.1	0.0	50	−19.2	0.7	3.2
Trades—W. Pacific Warm Pool Province	−16.2	0.0	27	−19.0	0.3	1.4
Trades—Archipelagic Deep Basins Province	−21.3	0.0	37	−19.3	0.9	3.7
Coastal—Alaska Downwelling Coastal Province	−20.8	1.5	31,38	−23.5	1.0	4.6
Coastal—California Upwelling Coastal Province	−19.0	2.1	31,39,40	−21.4	1.3	5.5
Coastal—Central American Coastal Province	−18.5	0.0	7	−18.4	0.6	2.5
Coastal—Chile-Peru Current Coastal Province	−19.6	1.6	41,50	−21.9	2.3	7.5
Coastal—China Sea Coastal Province	−19.3	0.3	42	−19.6	1.4	5.9
Coastal—East Australian Coastal Province	−21.3	0.3	43,44	−19.5	0.7	2.9
Coastal—New Zealand Coastal Province	−21.3	0.0	52	−22.2	1.3	4.7
Westerlies—S. Subtropical Convergence Province	−19.1	1.1	18,45,51	−21.8	1.0	6.5
Westerlies—Subantarctic Province	−24.2	0.2	2,46	−24.7	1.6	7.8
Polar—Antarctic Province	−27.5	1.0	2	−28.5	0.8	4.0
Polar—Austral Polar Province	−28.7	0.2	2,47,48	−29.2	0.5	2.8

Note: Reference numbers relate to the reference list in Appendix S4.

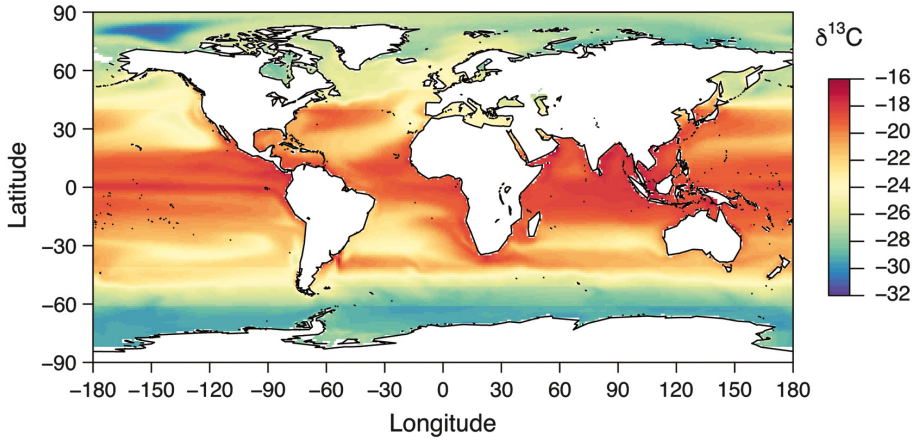

Fig. 1. Modeled annually averaged surface water distribution of the carbon isotope composition of phytoplankton ($\delta^{13}C_{PLK}$, ‰). Annual average $\delta^{13}C_{PLK}$ values are calculated using a monthly climatology for the period 2001–2010.

(mean ± SD: −27.2‰ ± 1.2‰) and reach most positive values of −28‰ to −26‰ at the edge of the subantarctic front and near the Antarctic shelf, and most negative values of −30‰ at the polar front (Fig. 1). In polar regions, annual average $\delta^{13}C_{PLK}$ values show an inter-hemispheric asymmetry, with overall more positive values in the Arctic Ocean than in the Antarctic Southern Ocean, with the exception of the margins of the Chukchi and Beaufort seas (Fig. 1). These predicted broad-scale spatial patterns are mostly explained by large-scale variations in the concentration and isotopic composition of dissolved CO_2, as well as growth rates and proportional abundance of key phytoplankton functional groups ("diatoms"- vs. "non-diatoms"-dominated phytoplankton communities), and co-vary with sea surface temperature.

Regional variations in annual average $\delta^{13}C_{PLK}$ values are super-imposed on the broad-scale latitudinal isotopic gradients described above (Fig. 1). In general, annual average $\delta^{13}C_{PLK}$ values are relatively positive in the Gulf Stream current, at the subtropical convergence, and in upwelling areas. By contrast, annual average $\delta^{13}C_{PLK}$ values are relatively negative in oligotrophic areas, where nutrients restrict phytoplankton growth, such as subtropical gyres (Figs. 1 and 2). Modeled annual average $\delta^{13}C_{PLK}$ values are also relatively negative in the Mediterranean Sea, presumably reflecting low phytoplankton growth rates within NEMO-MEDUSA (Figs. 1 and 2). These predicted regional-scale patterns are mostly explained by smaller-scale, often seasonal changes in the physiological correlates of phytoplankton communities, such as growth rates and proportional abundance of large- and small-celled phytoplankton (Fig. 2). As stated above, predictions of phytoplankton growth rates within ocean biogeochemical models are challenging, and consequently, predictions of regional growth rate-dependent variations in $\delta^{13}C_{PLK}$ values are relatively uncertain.

Validation

Comparing measured and modeled $\delta^{13}C_{PLK}$ values across Longhurst provinces shows close agreement, with a linear slope approximating 1. Mean (standard deviation) linear regression parameters from 500 iterations accounting for variances in the measured and modeled data are: $\delta^{13}C_{PLK} = 0.85\ (0.15) \times \delta^{13}C_{ZPLK} - 3.6\ (3.1)$ ($R^2 = 0.44$; P-value <0.001; Fig. 3A). Thus, the mean slope lies within one standard deviation of a unit line. The median residual standard error associated with any single predicted value was 2.2‰. Predicted $\delta^{13}C_{PLK}$ values are on average ~3.5‰ more negative than measured $\delta^{13}C_{ZPLK}$ values, which is within the range expected considering fractionation associated with increases in trophic level (Vander Zanden and Rasmussen 2001, McCutchan et al. 2003), and potential carnivory and omnivory in larger zooplankton. Modeled annual average $\delta^{13}C_{PLK}$ values reach more positive extreme values

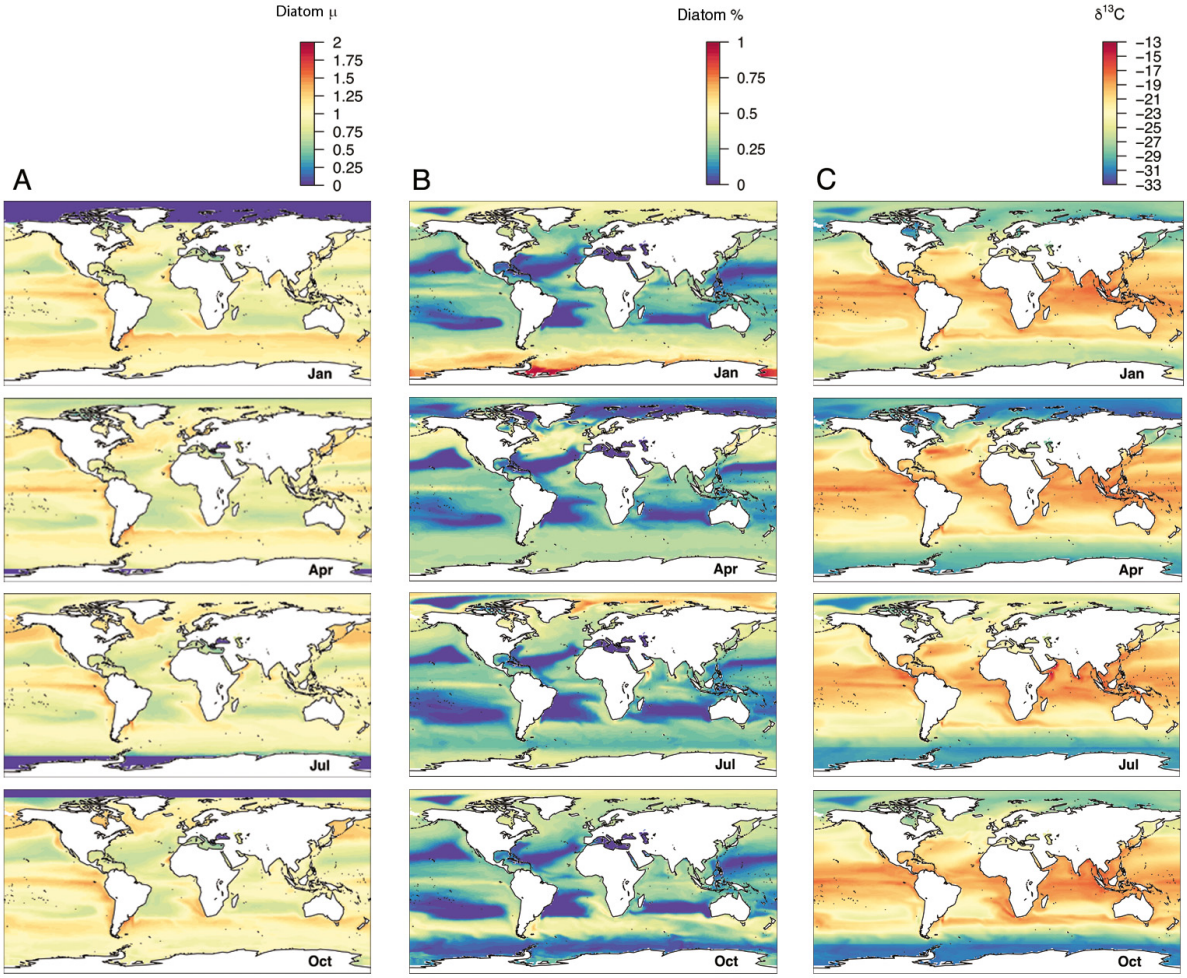

Fig. 2. Modeled monthly climatology distributions of (A) day-length corrected, scaled diatom growth rate (μ, number of divisions per day); (B) relative proportion of "diatoms" (vs. "non-diatoms"); (C) $\delta^{13}C_{PLK}$ values (‰). Diatom μ and proportion are simulated for the ocean's mixed layer by NEMO-MEDUSA. To highlight seasonality, outputs for January, April, July, and October for the period 2001–2010 are shown.

compared to measured $\delta^{13}C_{PLK}$ values, particularly in equatorial upwelling regions (Fig. 3B), although zooplankton in these regions is very sparsely sampled. Estimated annual average $\delta^{13}C_{PLK}$ values are more negative than measured $\delta^{13}C_{PLK}$ averages in the Boreal Polar Province due to very negative modeled $\delta^{13}C_{PLK}$ values in the Arctic Ocean north of the Chukchi Sea (Fig. 1); however, zooplankton sampling in this area is also limited. As indicated above, modeled annual average $\delta^{13}C_{PLK}$ values are also systematically negative compared to measured $\delta^{13}C_{ZPLK}$ values in the Mediterranean Sea, most likely because of underprediction of phytoplankton growth rates and possibly under-estimation of "diatom" relative abundance during winter months by NEMO-MEDUSA (Yool et al. 2013).

NEMO-MEDUSA is an open-ocean model that omits coastal processes such as run-off or littoral primary production, and our isotopic extension assumes that all carbon within the food web is derived from atmospheric CO_2. In littoral or coastal ecosystems, isotopically distinct carbon derived from terrestrial plants, macroalgae, and/or benthic remineralized sources can enter the food web, potentially influencing animal tissue isotopic compositions. Accordingly, we did not include zooplankton data recovered from estuarine or

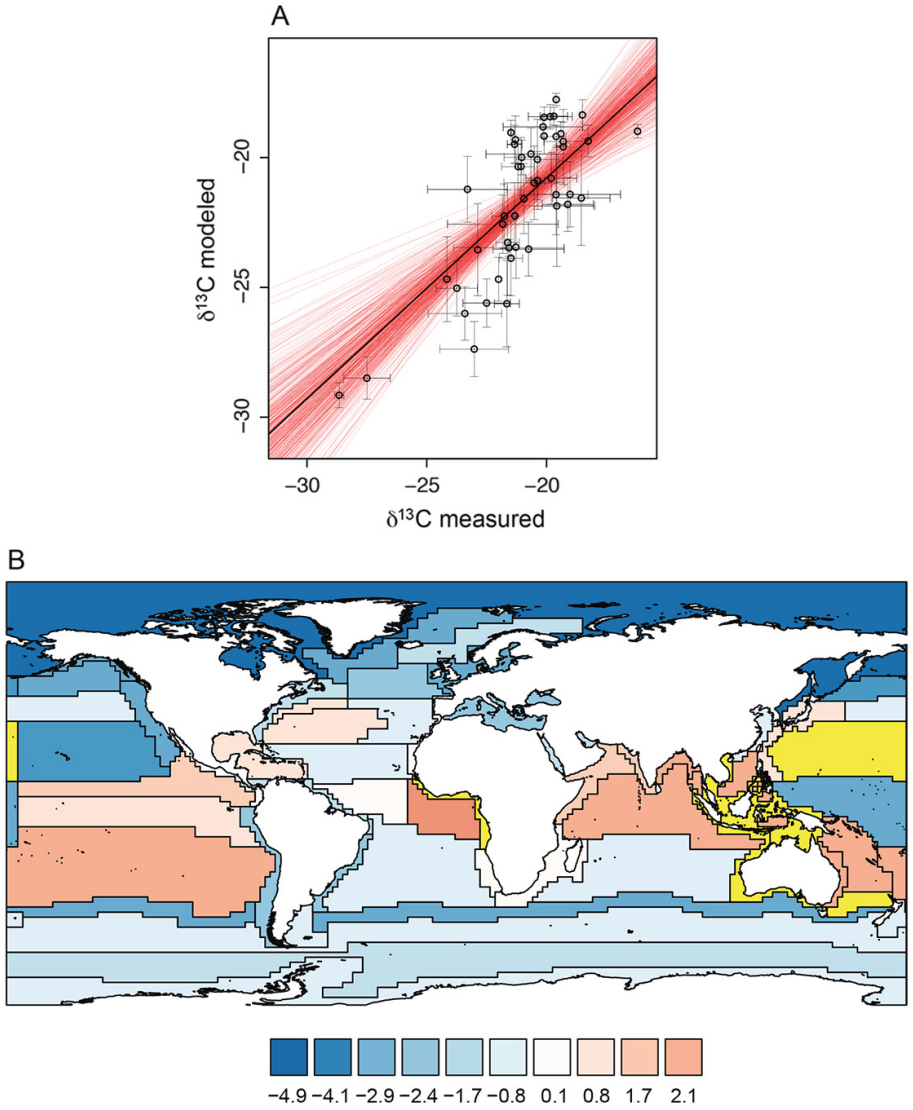

Fig. 3. Comparison of modeled $\delta^{13}C_{PLK}$ values from our carbon isotope model against measured $\delta^{13}C$ data for zooplankton ($\delta^{13}C_{ZPLK}$, ‰). (A) Estimated linear relationship between modeled annual average $\delta^{13}C_{PLK}$ and $\delta^{13}C_{ZPLK}$ values over Longhurst biogeographic provinces; red lines indicate 500 individual linear regression models each reflecting a random selection of 67% of Longhurst provinces with available data and accounting for modeled and measured variance within each province; the black line indicates the mean slope and intercept across the 500 iterations ($\delta^{13}C_{PLK} = 0.85 \times \delta^{13}C_{ZPLK} - 3.6$; $R^2 = 0.44$; P-value < 0.001). (B) Difference between mean modeled $\delta^{13}C_{PLK}$ and mean measured $\delta^{13}C_{ZPLK}$ values in each province (see Table 2); the yellow color indicates provinces for which no $\delta^{13}C_{ZPLK}$ data were available.

littoral systems in the data compilation. However, separating zooplankton data into Longhurst provinces defined as either coastal or open-ocean areas did not significantly influence the relationship between modeled and measured values. While this comparison is compromised by the limited abundance and sparse distribution of coastal zooplankton samples, mismatches between modeled and measured values in coastal and littoral areas may indicate incorporation of carbon from sources other than pelagic phytoplankton (e.g., continental-derived carbon).

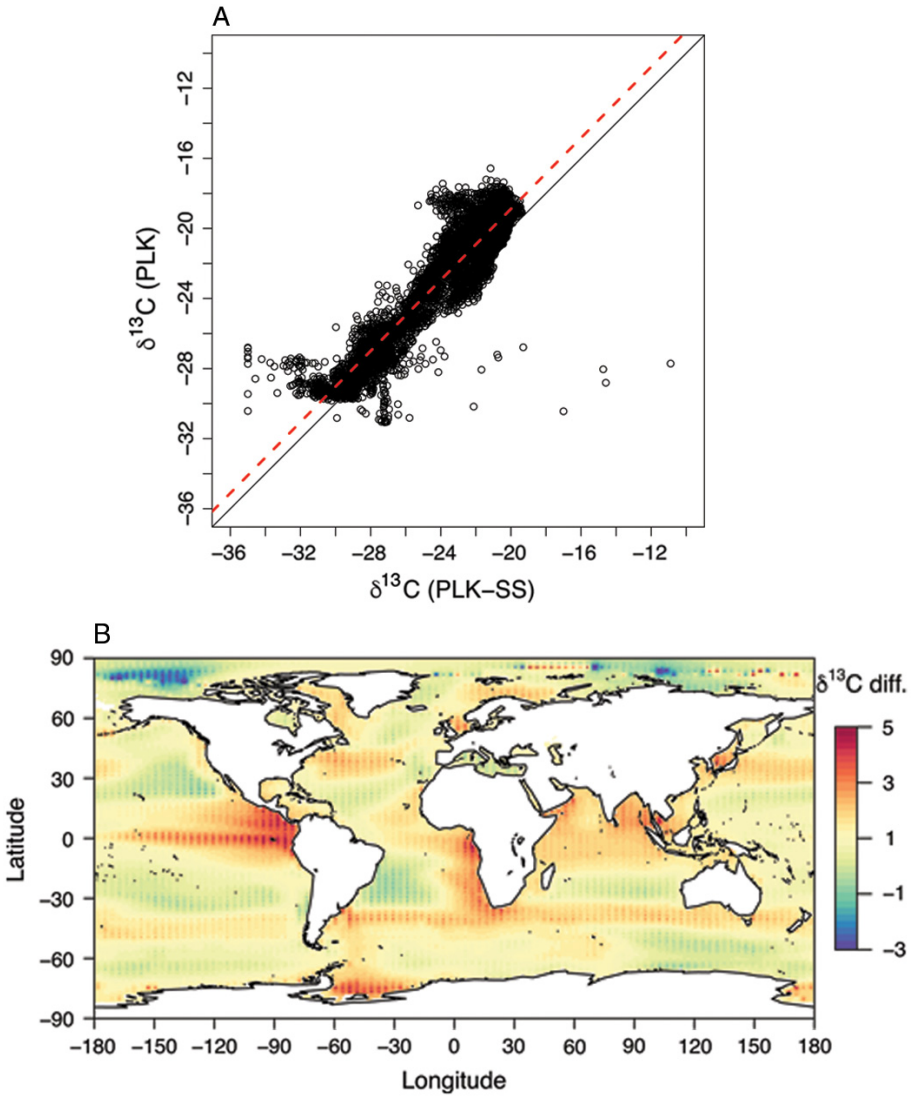

Fig. 4. Comparison of modeled $\delta^{13}C_{PLK}$ values from our offline carbon isotope model ($\delta^{13}C_{PLK}$) against modeled $\delta^{13}C_{PLK}$ values from the UVic earth system model ($\delta^{13}C_{PLK\text{-}SS}$, ‰; Schmittner and Somes 2016). (A) Estimated linear relationship between annual average $\delta^{13}C_{PLK}$ values (calculated using a monthly climatology for the period 2001–2010) and annual average $\delta^{13}C_{PLK\text{-}SS}$ values (for the model year 2010; $\delta^{13}C_{PLK} = 1.01 \times \delta^{13}C_{PLK\text{-}SS} + 1.5$, $R^2 = 0.78$, P-value <0.001) indicated by the red dotted line; the black line indicates the unit slope. (B) Difference between $\delta^{13}C_{PLK}$ and $\delta^{13}C_{PLK\text{-}SS}$ values interpolated by inverse distance weighting; mean difference across the global ocean was −0.55‰.

Despite differences in the underlying earth system models, the nature of isotopic incorporation into the models (online vs. offline isotopic extension), and differences in the variables influencing photosynthetic fractionation, there is strong agreement between our model and the UVic model (Schmittner and Somes 2016; Fig. 4). Simple linear regression between annual average $\delta^{13}C_{PLK}$ values predicted by our offline carbon isotope model and $\delta^{13}C$ values estimated by the UVic model ($\delta^{13}C_{PLK\text{-}SS}$) yielded a linear relationship with a slope approximating 1 ($\delta^{13}C_{PLK} = 1.01 \times \delta^{13}C_{PLK\text{-}SS} + 1.5$, $R^2 = 0.78$, P-value <0.001; Fig. 4A) and a mean residual standard error of

1.7‰. The close agreement between the two models reflects the first-order control on $\delta^{13}C_{PLK}$ values from surface water concentration and isotopic composition of dissolved CO_2. Annual average $\delta^{13}C_{PLK}$ values modeled within NEMO-MEDUSA were on average 1‰ more positive than those predicted by the UVic model. Values modeled within NEMO-MEDUSA also showed higher regional variability, presumably due to the influence of variable phytoplankton growth rates on fractionation during photosynthesis within the MEDUSA model, but not within the UVic model. Accordingly, $\delta^{13}C_{PLK}$ values predicted within MEDUSA were more positive in temperate regions and upwelling areas where phytoplankton growth rates are high, and relatively negative in subtropical gyres where phytoplankton growth is nutrient-limited (Fig. 4B).

Temporal variability in $\delta^{13}C_{PLK}$ values

Our carbon isotope model allows the prediction of temporal patterns in $\delta^{13}C_{PLK}$ values, and thus the construction of temporally explicit isoscapes, providing isoscapes for a specific point in time, or isoscapes integrated over a defined period. Temporally explicit isoscape modeling also provides an estimate of the intra- and inter-annual range in baseline carbon isotopes for the global ocean or any given basin. In the Atlantic Ocean, for instance, the predicted intra-annual range in $\delta^{13}C_{PLK}$ reaches ~10–12‰ in high and temperate latitudes and upwelling regions characterized by strong, transient phytoplankton blooms, and is limited to 0–2‰ in areas typified by relatively constant temperature and phytoplankton growth rates throughout the year, such as the tropics and subtropical gyres (Fig. 5; for inter-annual range in $\delta^{13}C_{PLK}$ values, see Appendix S2: Fig. S3). These predicted temporal patterns are influenced by relatively localized seasonal changes in phytoplankton growth rates and proportional abundance of "diatoms" and "non-diatoms" (Fig. 2). The high intra-annual variability in $\delta^{13}C_{PLK}$ values at high and temperate latitudes in the Northern Hemisphere reflects, for instance, the strong seasonal variability in phytoplankton growth rates (and concentration of dissolved CO_2) typical of "diatom" blooms (Fig. 2). The reduced variability in $\delta^{13}C_{PLK}$ values at comparable latitudes in the Southern

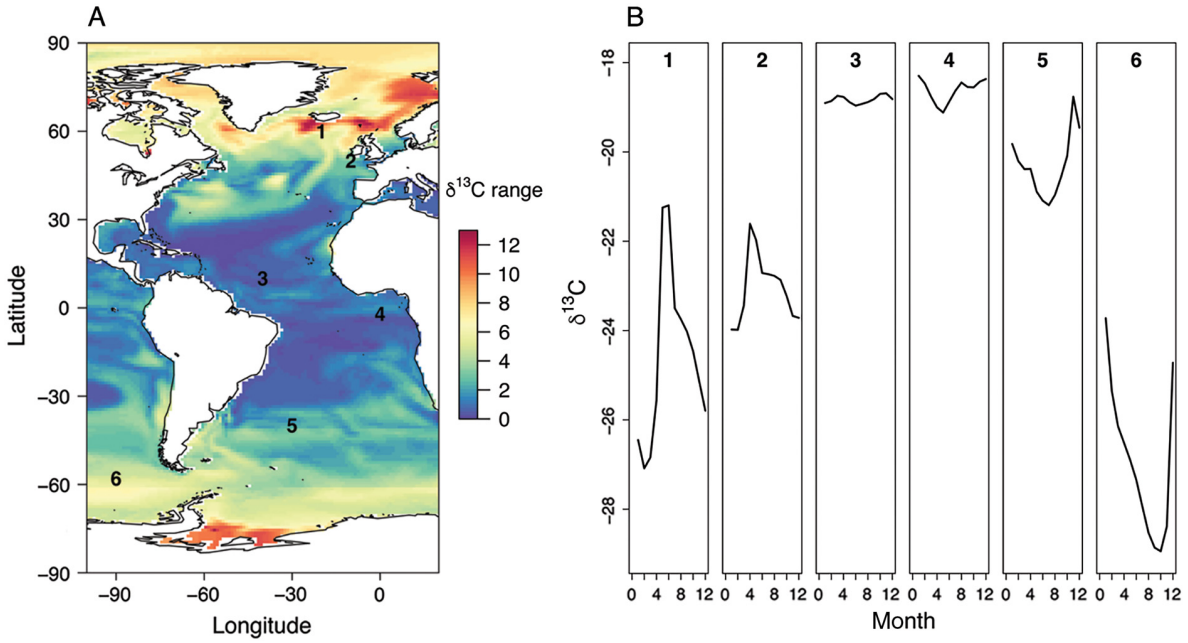

Fig. 5. Modeled temporal intra-annual variability in $\delta^{13}C_{PLK}$ values (‰): (A) intra-annual range in $\delta^{13}C_{PLK}$ values across the Atlantic Ocean; (B) time-series of monthly climatology $\delta^{13}C_{PLK}$ values at six locations along a latitudinal gradient, as indicated by numbers in A). Intra-annual range of $\delta^{13}C_{PLK}$ values is calculated as the range of monthly climatology $\delta^{13}C_{PLK}$ values.

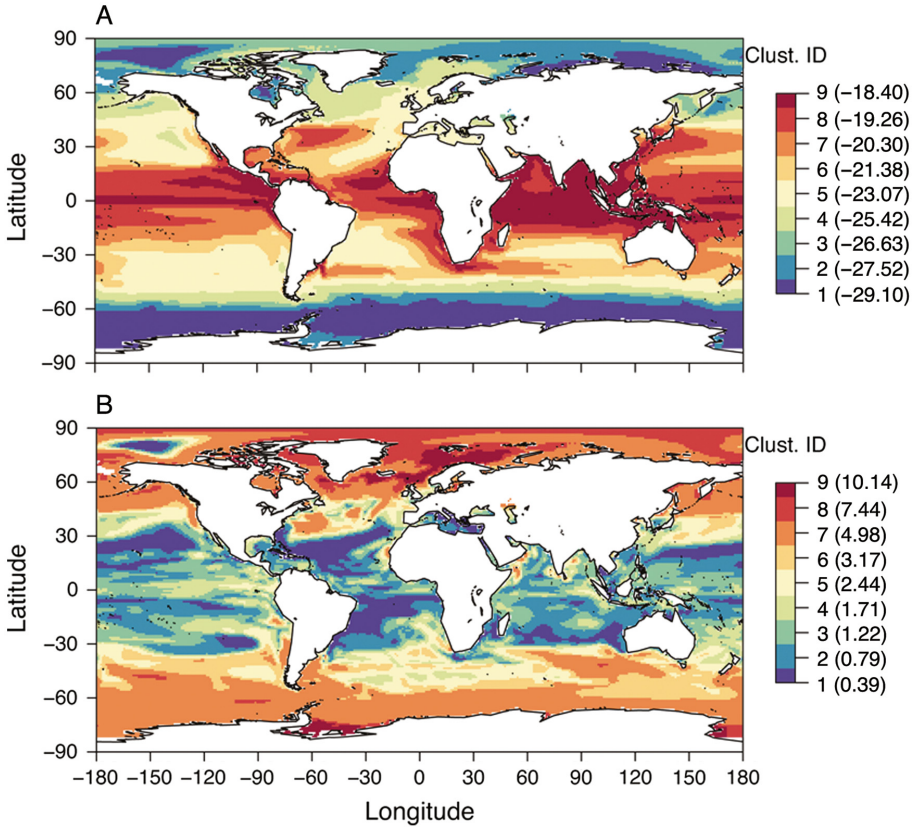

Fig. 6. Discrete isoscapes showing cluster ID for nine clusters of similar (A) annual average $\delta^{13}C_{PLK}$ grid cell values and (B) intra-annual range (i.e., difference between maximum and minimum value) in $\delta^{13}C_{PLK}$ grid cell values; numbers in brackets are mean annual average and range $\delta^{13}C_{PLK}$ values within each cluster. Both annual average and intra-annual range in $\delta^{13}C_{PLK}$ values are calculated using a monthly climatology for the period 2001–2010. For standard deviations of $\delta^{13}C_{PLK}$ values within each cluster, see Appendix S2: Fig. S4.

Ocean corresponds to lower overall growth rates throughout the year characteristic of high nutrient low chlorophyll zones, despite "diatom" blooms in the austral summer (Fig. 2).

Discussion

The main goal of this study was to develop a relatively simple, offline carbon isotope model to predict the spatio-temporal distributions of the carbon isotope composition of phytoplankton (here expressed as $\delta^{13}C_{PLK}$) at regional to global scales. To develop this model, we applied a basic function estimating carbon isotope fractionation during photosynthesis (ε_p; Rau et al. 1996, 1997) to ecological variables (i.e., sea surface temperature, concentration of dissolved CO_2, growth rates, and proportional abundance of key phytoplankton functional groups) predicted by the NEMO-MEDUSA coupled physics–biogeochemistry model (Yool et al. 2013). Our simplified model reproduces major spatial patterns in baseline carbon isotopes as observed in nature (Fig. 3), and agrees closely with models involving explicit parameterization of ^{12}C and ^{13}C through the underlying biogeochemical model (Schmittner et al. 2013, Schmittner and Somes 2016; Fig. 4).

Our carbon isotope model also allows the prediction of temporal variation in baseline carbon isotopes, and thus the construction of temporally explicit isoscapes (Fig. 2C), as well as time-integrated maps of the likely intra- and inter-annual ranges in $\delta^{13}C_{PLK}$ values (Figs. 5A and Appendix S2: Fig. S3A; see also Figs. 6B, 7B,

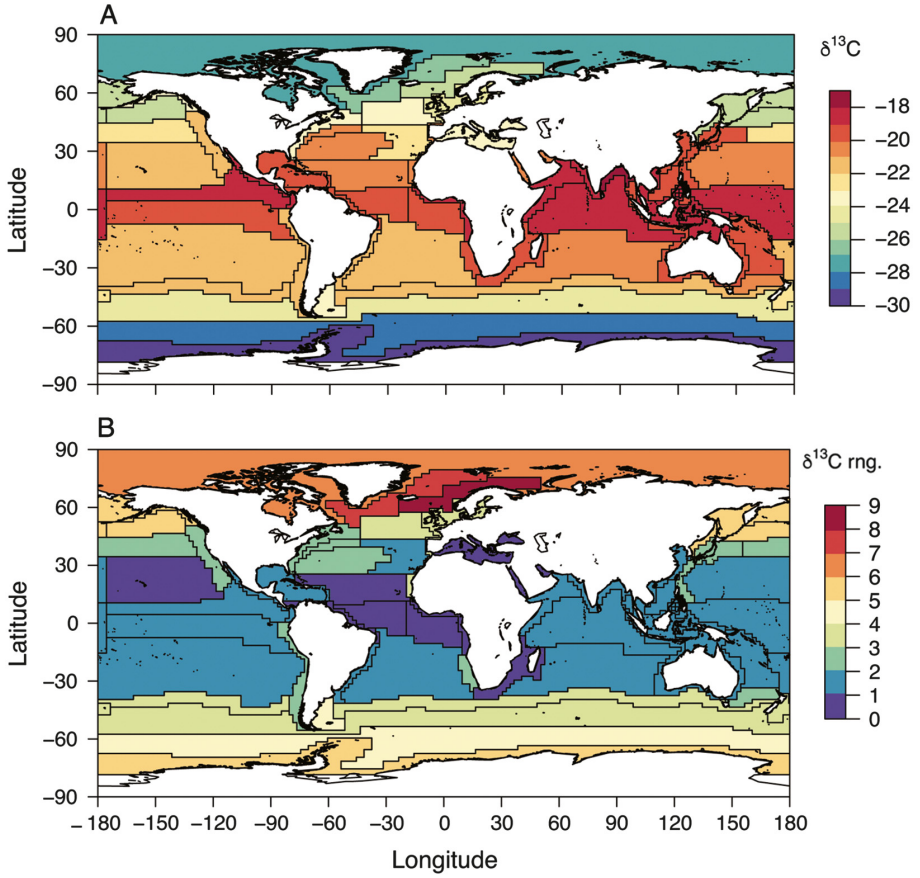

Fig. 7. Discrete isoscapes across Longhurst biogeographic provinces (Longhurst 1995, 1998, 2006): (A) mean annual average and (B) mean intra-annual range in $\delta^{13}C_{PLK}$ grid cell values within each province. Both annual average and intra-annual range in $\delta^{13}C_{PLK}$ values are calculated using a monthly climatology for the period 2001–2010. For standard deviations of $\delta^{13}C_{PLK}$ values within each province, see Appendix S2: Fig. S5.

Appendix S2: Figs. S6A and S7A). Explicit validation of predicted temporal variability in $\delta^{13}C_{PLK}$ values is, however, even more difficult than validation of geographic variance, particularly over large spatial scales. To our knowledge, a few studies have measured baseline carbon isotope values in open-ocean settings at a relatively high temporal resolution (Fry and Wainright 1991, Dehairs et al. 1997), and measurements were all taken at specific point locations usually within an area not larger than a grid cell. However, we argue that, if our parameterization of $\delta^{13}C_{PLK}$ reproduces broad-scale spatial patterns in baseline carbon isotopes, it should also be sufficient to recover broad-scale temporal baseline variations. Temporally explicit isoscapes may, in fact, be less uncertain than annual average isoscapes as annual average $\delta^{13}C_{PLK}$ values must be additionally weighted by the estimates of monthly production. Given the practical limitations concerning temporally explicit sampling in open-ocean conditions, mechanistic isotope models currently provide the best available tool to explore temporal variability in baseline carbon isotopes.

Model isoscapes' applications in marine ecology

Knowledge or prediction of temporal variations in baseline carbon isotopes may have important implications for the interpretation of animal tissue isotopic compositions for inferences on spatial and trophic ecology (Graham et al. 2010, Trueman et al. 2012, McMahon et al. 2013). The

transfer of temporal baseline variations to animal tissues generally decreases with decreasing tissue isotopic incorporation rate and increasing trophic level (Goering et al. 1990, Bump et al. 2007), potentially leading to the temporal averaging of substantial variability in baseline isotope values in high-trophic-level organisms. Within an organism, tissues with varying turnover rates will also inherit isotopic differences if the animal feeds in a region with high temporal variability in isotopic composition at the base of the food web. Migration across spatio-temporal isotopic gradients adds additional complexity to the interpretation of stable isotope compositions. Simulation modeling provides a tool to explore how spatio-temporal variability in $\delta^{13}C_{PLK}$ values is likely to affect tissue isotopic values.

We stress that modeled isoscapes are limited by the lack of suitable field validation datasets and by the simplifications and deficiencies implicit in both the biogeochemical and isotopic fractionation models. Here, comparison of predicted annual average $\delta^{13}C_{PLK}$ values against measured $\delta^{13}C$ data for zooplankton yields a mean residual standard error around any single point estimate of ~2‰, which is more than 10% of the total global range in $\delta^{13}C_{PLK}$ values (Fig. 1). Accordingly, we suggest that uncertainty inherent in modeled isoscapes is currently too large to permit explicit geographic assignments based on continuous isoscape surfaces (Wunder and Norris 2008, Wunder 2010). However, the relatively close agreement between modeled and measured estimates of mean $\delta^{13}C$ values in Longhurst biogeographic provinces implies that modeled ocean carbon isoscapes can provide a spatio-temporally explicit reference to which tissue isotopic compositions can be related. Modeled isoscape values can be partitioned to identify isotopically distinct regions within the global ocean (Fig. 6), or summarized to describe isotopic variability within biogeographically defined provinces (Longhurst 1995, 1998, 2006, Fig. 7). In both cases, spatial and temporal isotopic variability can be quantified within each discrete region and, if required, incorporated into geographic assignment algorithms (Wunder and Norris 2008, Wunder 2010, Vander Zanden et al. 2015, Trueman et al. 2016). Given that most marine oceanic animals are highly mobile, and have varying temporal isotopic incorporation rates, discrete isotopic provinces are likely to represent spatio-temporal variability in $\delta^{13}C_{PLK}$ values at scales more realistic and relevant to their spatial and temporal ecology.

Conclusions

1. Process-based carbon isotope models provide spatio-temporally explicit predictions of the carbon isotope composition of phytoplankton ($\delta^{13}C_{PLK}$) at the base of marine pelagic food webs. Modeled isoscapes reproduce major spatial patterns in baseline carbon isotope values as observed in nature and predicted by alternative models.
2. Our offline approach ensures that our model can be coupled to output from a wide range of alternative earth system models to explore mechanisms controlling and influencing distributions of $\delta^{13}C_{PLK}$ values in space and time. Mismatches between modeled and measured values may indicate the presence of additional carbon sources within food webs (especially in littoral settings), or may be used to compare the performance of competing ocean biogeochemical models.
3. Relatively accurate recovery of major spatial patterns in carbon isotopic baselines implies that modeled isoscapes also capture broad-scale temporal variations in $\delta^{13}C_{PLK}$ values; carbon isotope models provide the best currently available tool to explore temporal variability in baseline carbon isotope values.
4. Modeled isoscapes provide an estimate of the likely spatial and temporal variation in baseline carbon isotopes over a potential foraging range, and/or over a seasonal, annual, or multi-annual cycle; this variation can be explicitly included in statistical models of diet source partitioning or isotopic niche area, as well as taken into account when trying to interpret tissue isotopic compositions to gather information on location and movements.

Acknowledgments

We would like to thank the University of Southampton (Dean's award) for supporting this study as part of Sarah Magozzi's PhD research. We are also grateful to the National Science Foundation (Award no. 1137336)

for supporting Sarah Magozzi's participation to the Inter-university Training in Continental-scale Ecology Research-In-Residence Program at University of Colorado Denver, as well as Hannah Vander Zanden's postdoctoral fellowship through the ITCE Program (Award no. 1241286). We would also like to acknowledge Kelton W. McMahon and Christopher J. Somes for providing validation datasets. Finally, we would like to thank the reviewers for their valuable feedback on this paper.

Literature Cited

Barnes, C., S. Jennings, and J. T. Barry. 2009. Environmental correlates of large-scale spatial variation in the $\delta^{13}C$ of marine animals. Estuarine Coastal and Shelf Science 81:368–374.

Best, P. B., and D. M. Schell. 1996. Stable isotopes in southern right whale (*Eubalaena australis*) baleen as indicators of seasonal movements, feeding and growth. Marine Biology 124:483–494.

Bidigare, R. R., et al. 1997. Consistent fractionation of ^{13}C in nature and in the laboratory: growth-rate effects in some haptophyte algae. Global Biogeochemical Cycles 11:279–292.

Boecklen, W. J., C. T. Yarnes, B. A. Cook, and A. C. James. 2011. On the use of stable isotopes in trophic ecology. Annual Review of Ecology, Evolution, and Systematics 42:411–440.

Bowen, G. J. 2010*a*. Isoscapes: spatial pattern in isotopic biogeochemistry. Annual Review of Earth and Planetary Sciences 38:161–187.

Bowen, G. J. 2010*b*. Statistical and geostatistical mapping of precipitation water isotope ratios. Pages 139–160 *in* J. B. West, G. J. Bowen, T. E. Dawson, and K. P. Tu, editors. Isoscapes: understanding movement, pattern, and process on Earth through isotope mapping. Springer, Berlin, Germany.

Bowen, G. J., and J. Revenaugh. 2003. Interpolating the isotopic composition of modern meteoric precipitation. Water Resources Research 39:1299.

Bowen, G. J., L. I. Wassenaar, and K. A. Hobson. 2005. Global application of stable hydrogen and oxygen isotopes to wildlife forensics. Oecologia 143:337–348.

Bowen, G. J., and J. B. West. 2008. Isotope landscapes for terrestrial migration research. Pages 79–105 *in* K. A. Hobson and L. I. Wassenaar, editors. Tracking animal migration with stable isotopes. Academic Press, Amsterdam, The Netherlands.

Bump, J. K., K. Fox-Dobbs, J. L. Bada, P. L. Koch, R. O. Peterson, and J. A. Vucetich. 2007. Stable isotopes, ecological integration and environmental change: Wolves record atmospheric carbon isotope trend better than tree rings. Proceedings of the Royal Society B: Biological Sciences 274:2471–2480.

Burkhardt, S., U. Riebesell, and I. Zondervan. 1999. Stable carbon isotope fractionation by marine phytoplankton in response to daylength, growth rate, and CO_2 availability. Marine Ecology Progress Series 184:31–41.

Carpenter, E. J., H. R. Harvey, B. Fry, and D. G. Capone. 1997. Biogeochemical tracers of the marine cyanobacterium *Trichodesmium*. Deep-Sea Research Part I-Oceanographic Research Papers 44:27–38.

Cherel, Y., and K. A. Hobson. 2007. Geographical variation in carbon stable isotope signatures of marine predators: a tool to investigate their foraging areas in the Southern Ocean. Marine Ecology Progress Series 329:281–287.

Cherel, Y., K. A. Hobson, and H. Weimerskirch. 2000. Using stable isotope analysis of feathers to distinguish moulting and breeding origins of seabirds. Oecologia 122:155–162.

Choy, C. A., B. N. Popp, C. C. S. Hannides, and J. C. Drazen. 2015. Trophic structure and food resources of epipelagic and mesopelagic fishes in the North Pacific. Limnology and Oceanography 60:1156–1171.

Collins, W. J., et al. 2011. Development and evaluation of an Earth-system model – HadGEM2. Geoscientific Model Development Discussions 4:997–1062.

Cryan, P. M., C. A. Stricker, and M. B. Wunder. 2014. Continental-scale, seasonal movements of a heterothermic migratory tree bat. Ecological Applications 24:602–616.

Dehairs, F., E. Kopczynska, P. Nielson, C. Lancelot, D. C. E. Bakker, W. Koeve, and L. Goeyens. 1997. $\delta^{13}C$ of Southern Ocean suspended organic matter during spring and early summer: regional and temporal variability. Deep Sea Research Part II: Topical Studies in Oceanography 44:129–142.

Dunton, K. H., S. M. Saupe, A. N. Golikov, D. M. Schell, and S. V. Schonberg. 1989. Trophic relationships and isotopic gradients among Arctic and Subarctic marine fauna. Marine Ecology Progress Series 56:89–97.

Farquhar, G. D., M. H. O'Leary, and J. A. Berry. 1982. On the relationship between carbon isotope discrimination and the inter-cellular carbon dioxide concentration in leaves. Australian Journal of Plant Physiology 9:121–137.

Fischer, G., P. J. Muller, and G. Wefer. 1998. Latitudinal $\delta^{13}C_{org}$ variations in sinking matter and sediments from the South Atlantic: effects of anthropogenic CO_2 and implications for paleo-pCO_2 reconstructions. Journal of Marine Systems 17:471–495.

Flockhart, D. T. T., L. I. Wassenaar, T. G. Martin, K. A. Hobson, M. B. Wunder, and D. R. Norris. 2013. Tracking multi-generational colonization of the breeding grounds by monarch butterflies in eastern

North America. Proceedings of the Royal Society B: Biological Sciences 280:20101387.

Fontugne, M. R., and J. C. Duplessy. 1981. Organic carbon isotopic fractionation by marine plankton in the temperature range −1 to 31 °C. Oceanologica Acta 4:85–90.

Forsythe, W. C., E. J. Rykiel Jr., R. S. Stahl, H. Wu, and R. M. Schoofield. 1995. A model comparison for day-length as a function of latitude and day of the year. Ecological Modelling 80:87–95.

Fraley, C., A. E. Raftery, T. B. Murphy, and L. Scrucca. 2012. mclust version 4 for R: normal mixture modeling for model-based clustering, classification, and density estimation. Technical report No. 597. Department of Statistics, University of Washington, Seattle, Washington, USA.

Francois, R., M. A. Altabet, R. Goericke, D. C. McCorkle, C. Brunet, and A. Poisson. 1993. Changes in the $\delta^{13}C$ of surface water particulate organic matter across the subtropical convergence in the South West Indian Ocean. Global Biogeochemical Cycles 7:627–644.

Freeman, K. H., and J. M. Hayes. 1992. Fractionation of carbon isotopes by phytoplankton and estimates of ancient carbon dioxide levels. Global Biogeochemical Cycles 6:185–198.

Fry, B., and S. C. Wainright. 1991. Diatom sources of ^{13}C rich carbon in marine food webs. Marine Ecology Progress Series 76:149–157.

Garcia-Perez, B., and K. A. Hobson. 2014. A multi-isotope (δ^2H, $\delta^{13}C$, $\delta^{15}N$) approach to establishing migratory connectivity of Barn Swallow (*Hirundo rustica*). Ecosphere 5:1–12.

Goericke, R., and B. Fry. 1994. Variations of marine plankton $\delta^{13}C$ with latitude, temperature, and dissolved CO_2 in the world ocean. Global Biogeochemical Cycles 8:85–90.

Goericke, R., J. P. Montaya, and B. Fry. 1994. Physiology of isotope fractionation in algae and cyanobacteria. Pages 187–221 *in* K. Lajtha and B. Michener, editors. Stable isotopes in ecology and environmental science. Blackwell Scientific Publications, Oxford, UK; Boston, Massachusetts, USA.

Goering, J., V. Alexander, and N. Haubenstock. 1990. Seasonal variability of stable carbon and nitrogen isotope ratios of organisms in a North Pacific bay. Estuarine Coastal and Shelf Science 30:239–260.

Graham, B. S., P. L. Koch, S. D. Newsome, K. W. McMahon, and D. Aurioles. 2010. Using isoscapes to trace the movements and foraging behavior of top predators in oceanic ecosystems. Pages 299–318 *in* J. B. West, G. J. Bowen, T. E. Dawson, and K. P. Tu, editors. Isoscapes: understanding movement, pattern, and process on Earth through isotope mapping. Springer, Berlin, Germany.

Hinga, K. R., M. A. Arthur, M. E. Q. Pilson, and D. Whitaker. 1994. Carbon isotope fractionation by marine phytoplankton in culture – The effects of CO_2 concentration, pH, temperature, and species. Global Biogeochemical Cycles 8:91–102.

Hobson, K. A. 1999. Tracing origins and migration of wildlife using stable isotopes: a review. Oecologia 120:314–326.

Hobson, K. A., R. Barnett-Johnson, and T. Cerling. 2010. Using isoscapes to track animal migration. Pages 273–298 *in* J. B. West, G. J. Bowen, T. E. Dawson, and K. P. Tu, editors. Isoscapes: understanding movement, pattern, and process on Earth through isotope mapping. Springer, Berlin, Germany.

Hobson, K. A., D. X. Soto, D. R. Paulson, L. I. Wassenaar, and J. H. Matthews. 2012. A dragonfly δ^2H isoscape for North America: a new tool for determining natal origins of migratory aquatic emergent insects. Methods in Ecology and Evolution 3:766–772.

Hofmann, M., D. A. Wolf-Gladrow, T. Takahashi, S. C. Sutherland, K. D. Six, and E. Maier-Reimer. 2000. Stable carbon isotope distribution of particulate organic matter in the ocean: a model study. Marine Chemistry 72:131–150.

Jaeger, A., V. J. Lecomte, H. Weimerskirch, P. Richard, and Y. Cherel. 2010. Seabird satellite tracking validates the use of latitudinal isoscapes to depict predators' foraging areas in the Southern Ocean. Rapid Communications in Mass Spectrometry 24:3456–3460.

Jennings, S., and K. J. Warr. 2003. Environmental correlates of large-scale spatial variation in the $\delta^{15}N$ of marine animals. Marine Biology 142:1131–1140.

Jones, C. D., et al. 2011. The HadGEM2-ES implementation of CMIP5 centennial simulations. Geoscientific Model Development 4:543–570.

Keller, K., and F. M. M. Morel. 1999. A model of carbon isotopic fractionation and active carbon uptake in phytoplankton. Marine Ecology Progress Series 182:295–298.

Kelly, J. F. 2000. Stable isotopes of carbon and nitrogen in the study of avian and mammalian trophic ecology. Journal of Canadian Zoology 78:1–27.

Lara, R. J., V. Alder, C. A. Franzosi, and G. Kattner. 2010. Characteristics of suspended particulate organic matter in the southwestern Atlantic: influence of temperature, nutrient and phytoplankton features on the stable isotope signature. Journal of Marine Systems 79:199–209.

Laws, E. A., R. R. Bidigare, and B. N. Popp. 1997. Effect of growth rate and CO_2 concentration on carbon isotopic fractionation by the marine diatom

Phaeodactylum tricornutum. Limnology and Oceanography 42:1552–1560.

Laws, E. A., B. N. Popp, R. R. Bidigare, M. C. Kennicutt, and S. A. Macko. 1995. Dependence of phytoplankton carbon isotopic composition on growth rate and $CO_{2(aq)}$ – Theoretical considerations and experimental results. Geochimica Et Cosmochimica Acta 59:1131–1138.

Layman, C. A., et al. 2012. Applying stable isotopes to examine food-web structure: an overview of analytical tools. Biological Reviews 87:545–562.

Longhurst, A. R. 1995. Seasonal cycles of pelagic production and consumption. Progress in Oceanography 36:77–167.

Longhurst, A. R. 1998. Ecological geography of the sea. Academic Press, San Diego, California, USA.

Longhurst, A. R. 2006. Ecological geography of the sea. Second edition. Elsevier, Amsterdam, The Netherlands.

MacKenzie, K. M., C. Longmore, C. Preece, C. H. Lucas, and C. N. Trueman. 2014. Testing the long-term stability of marine isoscapes in shelf seas using jellyfish tissues. Biogeochemistry 121:441–454.

Madec, G., and the NEMO team. 2008. NEMO ocean engine. Note du Pole de modelisation. No. 27. Institut Pierre-Simon Laplace, France.

Maranon, E. 2009. Phytoplankton size structure. Pages 445–452 *in* J. H. Steele, K. Turekian, and S. Thorpe, editors. Encyclopedia of ocean sciences. Second edition. Academic Press, Amsterdam, The Netherlands.

McCutchan, J. H., W. M. Lewis, C. Kendall, and C. C. McGrath. 2003. Variation in trophic shift for stable isotope ratios of carbon, nitrogen, and sulfur. Oikos 102:378–390.

McMahon, K. W., L. L. Hamady, and S. R. Thorrold. 2013. A review of ecogeochemistry approaches to estimating movements of marine animals. Limnology and Oceanography 58:697–714.

Meehan, T. D., J. T. Giermakowski, and P. M. Cryan. 2004. GIS-based model of stable hydrogen isotope ratios in North American growing-season precipitation for use in animal movement studies. Isotopes in Environmental and Health Studies 40: 291–300.

Popp, B. N., E. A. Laws, R. R. Bidigare, J. E. Dore, K. L. Hanson, and S. G. Wakeham. 1998. Effect of phytoplankton cell geometry on carbon isotopic fractionation. Geochimica Et Cosmochimica Acta 62:69–77.

Popp, B. N., et al. 1999. Controls on the carbon isotopic composition of Southern Ocean phytoplankton. Global Biogeochemical Cycles 13:827–843.

Post, D. M. 2002. Using stable isotopes to estimate trophic position: models, methods, and assumptions. Ecology 83:703–718.

Radabaugh, K. R., D. J. Hollander, and E. B. Peebles. 2013. Seasonal $\delta^{13}C$ and $\delta^{15}N$ isoscapes of fish populations along a continental shelf trophic gradient. Continental Shelf Research 68:112–122.

Ramos, R., and J. Gonzalez-Solis. 2012. Trace me if you can: the use of intrinsic biogeochemical markers in marine top predators. Frontiers in Ecology and the Environment 10:258–266.

Rau, G. H., U. Riebesell, and D. WolfGladrow. 1996. A model of photosynthetic ^{13}C fractionation by marine phytoplankton based on diffusive molecular CO_2 uptake. Marine Ecology Progress Series 133:275–285.

Rau, G. H., U. Riebesell, and D. WolfGladrow. 1997. $CO_{2(aq)}$-dependent photosynthetic ^{13}C fractionation in the ocean: a model versus measurements. Global Biogeochemical Cycles 11:267–278.

Rau, G. H., R. E. Sweeney, and I. R. Kaplan. 1982. Plankton ^{13}C-^{12}C ratio changes with latitude – Differences between northern and southern oceans. Deep-Sea Research Part I-Oceanographic Research Papers 29:1035–1039.

Rau, G. H., T. Takahashi, D. J. Desmarais, D. J. Repeta, and J. H. Martin. 1992. The relationship between $\delta^{13}C$ of organic matter and $CO_{2(aq)}$ in ocean surface water – Data from a JGOFS site in the northeast Atlantic Ocean and a model. Geochimica Et Cosmochimica Acta 56:1413–1419.

Rau, G. H., T. Takahashi, and D. J. D. Marais. 1989. Latitudinal variations in plankton $\delta^{13}C$ – Implications for CO_2 and productivity in past oceans. Nature 341:516–518.

Rundel, C. W., et al. 2013. Novel statistical methods for integrating genetic and stable isotope data to infer individual-level migratory connectivity. Molecular Ecology 22:4163–4176.

Sackett, W. M., W. R. Eckelman, M. L. Bender, and A. W. H. Be. 1965. Temperature dependence of carbon isotope composition in marine plankton and sediments. Science 148:235–237.

Saupe, S. M., D. M. Schell, and W. B. Griffiths. 1989. Carbon isotope gradients in western Arctic zooplankton. Marine Biology 103:427–432.

Schell, D. M., B. A. Barnett, and K. A. Vinette. 1998. Carbon and nitrogen isotope ratios in zooplankton of the Bering, Chukchi and Beaufort seas. Marine Ecology Progress Series 162:11–23.

Schell, D. M., S. M. Saupe, and N. Haubenstock. 1989. Bowhead whale (*Balaena mysticetus*) growth and feeding as estimated by $\delta^{13}C$ techniques. Marine Biology 103:433–443.

Schmittner, A., N. Gruber, A. C. Mix, R. M. Key, A. Tagliabue, and T. K. Westberry. 2013. Biology and air-sea gas exchange controls on the distribution of carbon isotope ratios ($\delta^{13}C$) in the ocean. Biogeosciences 10:5793–5816.

Schmittner, A., and C. J. Somes. 2016. Complementary constraints from carbon (^{13}C) and nitrogen (^{15}N) isotopes on the Glacial Ocean's soft-tissue biological pump. Paleoceanography 31:669–693.

Somes, C. J., A. Schmittner, E. D. Galbraith, M. F. Lehmann, M. A. Altabet, J. P. Montoya, R. M. Letelier, A. C. Mix, A. Bourbonnais, and M. Eby. 2010. Simulating the global distribution of nitrogen isotopes in the ocean. Global Biogeochemical Cycles 24:GB4019.

Tagliabue, A., and L. Bopp. 2008. Towards understanding global variability in ocean carbon-13. Global Biogeochemical Cycles 22:GB1025.

Timmermann, R., H. Goosse, G. Madec, T. Fichefet, C. Ethe, and V. Duliere. 2005. On the representation of high latitude processes in the ORCA-LIM global coupled sea ice-ocean model. Ocean Modelling 8:175–201.

Trueman, C. N., G. Johnston, B. O'Hea, and K. M. MacKenzie. 2014. Trophic interactions of fish communities at midwater depths enhance long-term carbon storage and benthic production on continental slopes. Proceedings of the Royal Society B 281:20140669.

Trueman, C. N., K. M. MacKenzie, and M. R. Palmer. 2012. Identifying migrations in marine fishes through stable isotope analysis. Journal of Fish Biology 81:826–847.

Trueman, C. N., K. M. MacKenzie, K. St, and J. Glew. 2016. Stable isotope-based location in a shelf sea setting: Accuracy and precision are comparable to light-based location methods. Methods in Ecology and Evolution 8:232–240.

Van Wilgenburg, S. L., and K. A. Hobson. 2011. Combining stable-isotope (δD) and band recovery data to improve probabilistic assignments of migratory birds to origin. Ecological Applications 21:1340–1352.

Van Wilgenburg, S. L., K. A. Hobson, K. R. Brewster, and J. M. Welker. 2012. Assessing dispersal in threatened migratory birds using stable hydrogen isotope (δD) analysis of feathers. Endangered Species Research 16:17–29.

Vander Zanden, M. J., and J. B. Rasmussen. 2001. Variation in $\delta^{15}N$ and $\delta^{13}C$ trophic fractionation: implications for aquatic food web studies. Limnology and Oceanography 46:2061–2066.

Vander Zanden, H. B., et al. 2015. Determining origin in a migratory marine vertebrate: a novel method to integrate stable isotopes and satellite tracking. Ecological Applications 25:320–335.

Vokhshoori, N. L., T. Larsen, and M. D. McCarthy. 2014. Reconstructing $\delta^{13}C$ isoscapes of phytoplankton production in a coastal upwelling system with amino acid isotope values of littoral mussels. Marine Ecology Progress Series 504:59–72.

Vokhshoori, N. L., and M. D. McCarthy. 2014. Compound-specific $\delta^{15}N$ amino acid measurements in littoral mussels in the California upwelling ecosystem: a new approach to generating baseline $\delta^{15}N$ isoscapes for coastal ecosystems. PLoS One 9:e98087.

Wassenaar, L. I. 2008. An introduction to light stable isotopes for use in terrestrial animal migration studies. Pages 21–44 *in* K. A. Hobson and L. I. Wassenaar, editors. Tracking animal migration with stable isotopes. Academic Press, Amsterdam, The Netherlands.

West, J. B., G. J. Bowen, T. E. Dawson, and K. P. Tu, editors. 2010. Isoscapes: understanding movement, pattern, and process on Earth through isotope mapping. Springer, Berlin, Germany.

Wong, W. W., and W. M. Sackett. 1978. Fractionation of stable carbon isotopes by marine phytoplankton. Geochimica Et Cosmochimica Acta 42:1809–1815.

Wunder, M. B. 2010. Using isoscapes to model probability surfaces for determining geographic origins. Pages 251–270 *in* J. B. West, G. J. Bowen, T. E. Dawson, and K. P. Tu, editors. Isoscapes: understanding movement, pattern, and process on Earth through isotope mapping. Springer, Berlin, Germany.

Wunder, M. B., and D. R. Norris. 2008. Analysis and design for isotope-based studies of migratory animals. Pages 107–128 *in* K. A. Hobson and L. I. Wassenaar, editors. Tracking animal migration with stable isotopes. Academic Press, Amsterdam, The Netherlands.

Yool, A., E. E. Popova, and T. R. Anderson. 2013. MEDUSA-2.0: an intermediate complexity biogeochemical model of the marine carbon cycle for climate change and ocean acidification studies. Geoscientific Model Development 6:1767–1811.

Zeebe, R. E., D. A. Wolf-Gladrow, and H. Jansen. 1999. On the time required to establish chemical and isotopic equilibrium in the carbon dioxide system in seawater. Marine Chemistry 65:135–153.

Supporting Information

Additional Supporting Information may be found online at: http://onlinelibrary.wiley.com/doi/10.1002/ecs2.1763/full